General Characteristics of Robust Orbit Insertion and Trajectory Design with MOI Robustness in MMX Mission

By Shota Takahashi,[1] Naoko Ogawa,[2] Yasuhiro Kawakatsu,[2]

[1]Department of Mechanical Engineering, Keio University, Japan
[2]Institute of Space and Astronautical Science, JAXA, Japan

Failure of the orbit insertion maneuver has significant impact on the entire mission, for the trajectory of a spacecraft is largely deflected by swing-by. One method to reduce the risk is to target a point on the B-plane where the spacecraft reaches the synchronous orbit with the target body in the case of insertion failure. We call this method robust orbit insertion. Among various failure modes at the orbit insertion maneuver, we focus on the robustness to the escape by inoperative maneuver. The impact parameters on the B-plane to achieve robust orbit insertion are formulated based on the geometry of velocity vectors at swing-by. To achieve robust orbit insertion, necessary deflection angle α_{robust} at swing-by must be smaller than the possible maximum deflection angle α_{max} for the target body. When the trajectory of a planet is approximated as a circular orbit, the relationship of α_{max} and α_{robust} is characterized by a single parameter λ. Using polar orbit insertion as an example, maps which show the reachability of synchronous orbit after the insertion failure for each approaching condition are presented. The derived maps can be used as a tool to asses the applicability of robust orbit insertion in the design phase of a mission scenario. As an application to practical mission design, we demonstrate the use of robust orbit insertion in JAXA's MMX mission.

Nomenclature

α	:	deflection angle at swing-by
β	:	angle between $v_{\infty in}$ and $-v_p$
$\hat{k}$	:	reference vector to represent orbital plane
$\hat{S}, \hat{T}, \hat{R}$	:	unit vectors for B-plane coordinate
b	:	norm of B vector
$D(\alpha)_n$	:	rotation matrix around n-th axis by angle α
λ	:	non-dimensional parameter
η	:	angle between v_p and v_{out}
μ	:	standard gravitational parameter
ψ	:	parameter to express $v_{\infty out}$
θ	:	angle from $\hat{T}$ axis to B
φ	:	angle that indicates the track of $v_{\infty out}$
φ_R	:	angle from $\hat{P_1}$ axis to $\hat{R}$ axis
a	:	semimajor axis
L_{sf}	:	scaling factor for length
T_{sf}	:	scaling factor for time
M	:	number of revolution by a target body
N	:	number of revolution by a spacecraft
T	:	orbital period
v_∞	:	hyperbolic excess velocity
δ	:	declination
ω	:	argument of periapsis
Subscripts		
p	:	planet
in	:	incoming
out	:	outgoing
S/C	:	spacecraft
peri	:	periapsis
Superscripts		
$*$	:	non-dimensional
^	:	unit vector

1.   Introduction

In the interplanetary exploration, the orbit insertion is one of the most critical event in the entire mission sequence. If an orbiter does not perform a maneuver to decelerate itself with respect to a target body, it flies by the target body and escapes into the deep space. This means the failure of the orbit insertion has strong impact on the outcome of the mission.

Generally, there are a lot of failure modes in the orbit insertion maneuver. In the past NASA's NEAR Shoemaker mission, a temporal malfunction in the attitude control system while maneuvering caused a one-year delay of the rendezvous with an asteroid Eros.[1,2] In Japan, Venus exploration mission Akatsuki suffered from the insertion failure. The orbit maneuvering engine broke down amid the thrust, and achieved ΔV was only 20% of its nominal value.[3] In order to assess the possibility of each failure mode, consideration of thruster and spacecraft systems will be necessary. In this study, we only focus on the failure mode that the spacecraft cannot perform any maneuver and escape into the deep space.

As a measure to avoid the risk, utilization of the synchronous orbit has been proposed.[4] The idea is to target a point on the B-plane so that a spacecraft enters a synchronous orbit with the body when the maneuver for insertion fails. If a spacecraft is on the synchronous orbit, the spacecraft's and target body's revolution period around the primary body form a simple integer ratio, which materializes the re-encounter at the exact same location. We call this method robust orbit insertion and the condition to reach synchronous orbit robust condition, following the denomination in the preceding research. The previous work has focused only on the trajectory design for SELENE mission by JAXA. Thus, the motivation in this study is to investigate the applicability of the method in general. As a first step, we for-
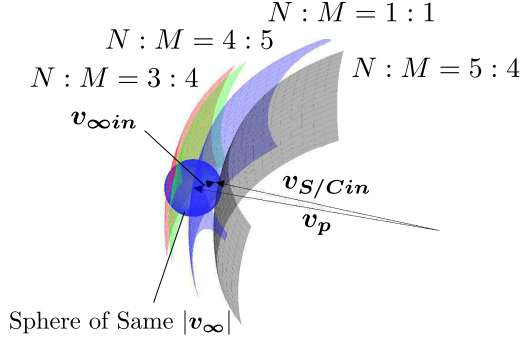
Fig. 1. 3D view of the velocity vector geometry at swing-by.

mulate the B-plane parameters b and θ necessary for the robust orbit insertion through geometric analysis on the velocity vectors at swing-by, which has not shown in the forgoing works.

Another contribution of this work is to systematically investigate the approaching condition that is advantageous for the robust orbit insertion. It is desirable that the robust condition corresponds to other mission requirements such as achieving small insertion ΔV or passing particular point over the target body. In the preceding study, a method to adjust the robust condition by the use of an intermediate Lunar swing-by has been exemplified. Introducing the intermediate swing-by is inconvenient if the target body has a large orbital period. Therefore, knowing the reasonable approaching condition a priori is beneficial in the design of an interplanetary trajectory. Using polar orbit insertion as an example, maps which show the reachability and information regarding insertion ΔV over the grid of approaching condition are presented.

To further evaluate if the method can be utilized in the practical mission design with a complex insertion sequence, the application to JAXA's MMX (Martian Moons eXploration) mission is studied. MMX is a sample return mission planned to be launched in the early 2020s. The spacecraft needs to perform multiple maneuvers for Mars orbit insertion (MOI), which insert the probe into the same orbit with one of the Martian moons Phobos. When we draw a contour of the distribution of ΔV for MOI on the B-plane, it shows a complex trend. The process to design a trajectory that satisfies mission requirements and the robust condition is discussed.

2. Geometric Analysis of Velocity Vectors

2.1. Velocity to Achieve Synchronous Orbit

We assume a target body and a primary body as a planet and Sun respectively for ease of explanation. The insertion to the synchronous orbit after the swing-by is realized in other systems such as Earth-Moon system in the same manner. As for the swing-by trajectory where a spacecraft naturally returns to the same body after a certain time of flight, the exhaustive research has been conducted in the framework of two-body problem.[5] Of the possible free-return trajectories presented in the research, we focus only on the full-revolution trajectories. The synchronous orbit with the target body satisfies the following relationship.

$$T_{S/C} = \frac{M}{N} T_p \tag{1}$$

where N and M are irreducible. A spacecraft can re-encounter the target body at the same location after the period of MT_p in the case of insertion failure. Fig. 1 shows the relationship among velocity vectors at the swing-by. Since $|v_{\infty in}|$ equals $|v_{\infty out}|$, the vector $v_{\infty out}$ is somewhere on the sphere with radius $|v_\infty|$. When $v_{\infty out}$ is at the intersection of $|v_\infty|$ sphere and the sphere whose radius is expressed in equation Eq. (2), the necessary condition for the robust orbit insertion is met.

$$v_{out} = \sqrt{\mu_{Sun}\left(\frac{2}{r_p} - \left(\frac{N}{M}\right)^{\frac{2}{3}}\frac{1}{a_p}\right)} \tag{2}$$

2.2. B-plane parameters for Robust Orbit Insertion

Several formulas and coordinate systems are proposed to help design swing-by trajectories.[6,7] They are useful when we design various variables at the same time such as orbital period, inclination, eccentricity, etc. However, our objective is to find the relation between B-plane parameters and orbital period; therefore, new reference frames are introduced. Figs. 2 and 3 show the definition of angles and coordinate systems associated with the velocity vectors. The point O_1 is the origin of the velocity vectors viewed from the primary, whereas the point O_2 is the origin of the velocity vectors viewed from the planet. The orthogonal coordinate system $O_2 - q_1 q_2 q_3$ and $O_2 - P_1 P_2 P_3$ are defined. The direction of q_1 is same with v_p. The direction of q_2 and P_1 is same with $v_{in} \times v_p$ direction. P_2 is aligned with $v_{\infty in}$. The vector $v_{\infty out}$ comes at the intersection of v_∞ sphere and the sphere of $|v_{out}|$. The two spheres form a circle, and we can designate a $v_{\infty out}$ by a single parameter ψ as in Fig. 4.

$$v_{\infty out} = \begin{pmatrix} L \\ V\sin\psi \\ V\cos\psi \end{pmatrix} \tag{3}$$

L and V is expressed as follows.

$$L = v_{out}\cos\eta - v_p \tag{4}$$

$$V = v_{out}\sin\eta \tag{5}$$

$$\text{here} \quad \eta = \arccos\left(\frac{v_p^2 + v_{out}^2 - v_\infty^2}{2v_p v_{out}}\right) \tag{6}$$

By rotating the coordinate system, the expression for $v_{\infty out}$ in $O_2 - P_1 P_2 P_3$ coordinate system is derived.

$$v_{\infty out} = D(\beta)_1 D(\pi/2)_3 \begin{pmatrix} L \\ V\sin\psi \\ V\cos\psi \end{pmatrix}$$
$$= \begin{pmatrix} V\sin\psi \\ V\sin\beta\cos\psi - L\cos\beta \\ L\sin\beta + V\cos\beta\cos\psi \end{pmatrix} \tag{7}$$

From this equation, a deflection angle α after the swing-by for each parameter ψ is obtained.

$$2\alpha = \arccos\left(\frac{v_{\infty in} \cdot v_{\infty out}}{v_\infty^2}\right)$$
$$= \arccos\left(\frac{V\sin\beta\cos\psi - L\cos\beta}{v_\infty}\right) \tag{8}$$

The angle φ is defined as shown in Fig. 5 to correlate ψ to B-plane parameter θ. The angle φ is measured from P_1 axis
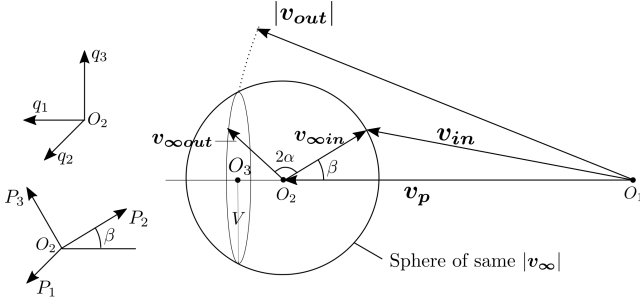
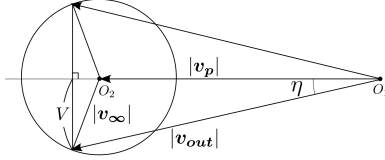Fig. 2. Relationship among velocity vectors at the swing-by

Fig. 3. Two-dimensional geometry of velocity vectors at the swing-by

to a mapped trace of $v_{\infty out}$ on the $P_1 P_3$ plane. From Eq. (7), parameter φ that corresponds to each ψ is derived as

$$\cos \varphi = \frac{V \sin \psi}{\sqrt{(V \sin \psi)^2 + (L \sin \beta + V \cos \beta \cos \psi)^2}}$$
$$\sin \varphi = \frac{L \sin \beta + V \cos \beta \cos \psi}{\sqrt{(V \sin \psi)^2 + (L \sin \beta + V \cos \beta \cos \psi)^2}} \quad (9)$$

To associate B-plane coordinate system with $O_2 - P_1 P_3$ coordinate system, we introduce another parameter φ_R. As shown in the bottom right picture in Fig. 5, φ_R is determined from the following equations

$$\cos \varphi_R = \hat{R} \cdot \hat{P_1}$$
$$\sin \varphi_R = \hat{R} \cdot \hat{P_3} \quad (10)$$

and then θ for each parameter ψ is computed as

$$\theta = \frac{3}{2} \pi + \varphi_R - \varphi \quad (11)$$
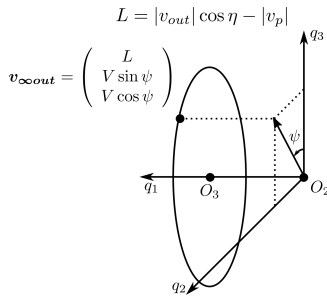

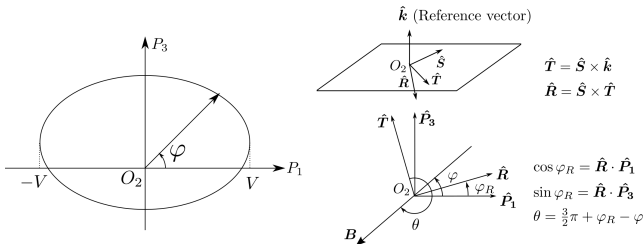Fig. 4. $v_{\infty out}$ in $O_2 - q_1 q_2 q_3$ coordinate system

Fig. 5. Mapping of $v_{\infty out}$ onto $P_1 P_3$ plane

The value of b is calculated from Eqs. (8), (12), and (13).

$$\sin \alpha = \frac{1}{1 + \frac{r_{peri} v_\infty^2}{\mu_p}} \quad (0° \le \alpha \le 90°) \quad (12)$$

$$b = r_{peri} \sqrt{1 + \frac{2\mu_p}{r_{peri} v_\infty^2}} \quad (13)$$

3. General Characteristics of Robust Orbit Insertion

3.1. Reachability of Resonant Orbit

How acutely the body can bend spacecraft's trajectory depends on R_p and μ_p. Smaller radius enables close approach to the mass center, and body with larger μ_p can bend the trajectory more easily, both of which lead to the increase in possible maximum deflection angle at the swing-by. Whether we can use the method of robust insertion depends on the deflection angle α_{robust} and α_{max} at a given approaching velocity. In this section, we generally characterize the reachability of the synchronous orbit after a swig-by. To make the system time independent, the velocity of the planet is assumed to be constant; the velocity of each planet is computed as a velocity of circular orbit with radius a_p. This assumption becomes valid when the eccentricity of the planet is close to zero.

3.2. Scaling

When we choose scaling factor for nondimensionalization as follows, α_{max} and α_{robust} are characterized by a single parameter associated with the target body.

$$L_{sf} = R_p \quad \text{(radius of the target body)}$$

$$T_{sf} = \sqrt{\frac{R_p^3}{\mu_p}}$$

The upper bound is given as

$$\alpha_{max} = \arcsin \left(\frac{1}{1 + v_\infty^2} \right) \quad (14)$$

and α_{robust} is obtained from the following equations.

$$2\alpha_{robust} = \arccos \left(\frac{V^* \sin \beta \cos \psi - L^* \cos \beta}{v_\infty^*} \right) \quad (15)$$

$$\cos \eta = \frac{v_{out}^{*2} + v_p^{*2} - v_\infty^{*2}}{2 v_{out}^* v_p^*} \quad (16)$$

$$\sin \eta = \sqrt{1 - \cos \eta^2} \quad (17)$$

$$V^* = v_{out}^* \sin \eta \quad (18)$$

$$L^* = v_{out}^* \cos \eta - v_p^* \quad (19)$$

$$v_{out}^* = \sqrt{\lambda \left(2 - \left(\frac{N}{M} \right)^{\frac{2}{3}} \right)} \quad (20)$$

$$v_p^* = \sqrt{\lambda} \quad (21)$$

$$\lambda = \frac{R_p \mu_{Sun}}{a_p \mu_p} \quad (22)$$

The parameter λ defined in Eq. (22) becomes square of the ratio of the velocity of the planet to the first astronautical velocity around the planet. A small λ corresponds to a large first

Table 1. Body name and corresponding parameter λ

Target	Primary	λ	v_∞^* for Hohmann transfer from Earth
Moon	Earth	3.67×10^{-1}	3.89×10^{-1} (from LEO)
Mercury	Sun	2.54×10^2	3.20
Venus	Sun	2.28×10	3.70×10^{-1}
Earth	Sun	1.42×10	-
Mars	Sun	4.62×10	7.46×10^{-1}
Jupiter	Sun	9.62×10^{-2}	1.34×10^{-1}
Saturn	Sun	1.48×10^{-1}	2.17×10^{-1}
Uranus	Sun	2.04×10^{-1}	3.09×10^{-1}
Neptune	Sun	1.07×10^{-1}	2.44×10^{-1}

Fig. 6. Reachability of robust orbit insertion over v_∞ and angle β for Mars. $\lambda = 46.2$ and $\varphi_R = 45$deg.

astronautical velocity for a given v_p. If the first astronautical velocity is relatively large, a spacecraft can attain high speed at the periapsis for a same v_∞, which results in the large α_{max}. Therefore, λ signifies how hard it is to deflect the trajectory of a spacecraft. We can use the robust orbit insertion if the condition $\alpha_{robust} \le \alpha_{max}$ is satisfied.

3.3. Robust Polar Orbit Insertion

When we plan an orbit insertion, its target trajectory is decided so that the trajectory meets mission requirements and, at the same time, has small ΔV. It is conceivable that there is a trade-off between the condition for the robust insertion and required ΔV. With an intent to evaluate the trade-off in a general manner, an orbit insertion to polar orbit is discussed in this section.

The reason we choose a polar orbit as a test case is that its simple formulation is suitable for investigating general characteristics of the robust orbit insertion. When a spacecraft approaches a target body, there are always regions that we can insert a spacecraft into the polar orbit, regardless of its approaching direction. For instance, if a reference vector that defines the B-plane is in a direction of the north pole, targeting any point on the $\hat{R}$ axis results in the insertion to the polar orbit. The study on the polar orbit insertion is also useful from the viewpoint of actual mission application. In a planetary exploration mission, the polar orbit is often profitable, for a spacecraft observes the entire surface of the body as a result of its rotation.

The robust orbit insertion to the polar orbit is characterized by the geometric parameter φ_R defined in Eq. (10). The parameter φ_R indicates the direction of the south pole in P_1P_3 plane when we choose $\hat{k}$ as a normal vector of equatorial plane. By solving Eq. (7) for ψ, we can find ψ_R corresponding to φ_R ($-\pi/2 < \varphi_R < \pi/2$). Derived equation is

$$-V\cos\beta\cos\psi_R + V\tan\varphi_R\sin\psi_R = L\sin\beta \qquad (23)$$

and the solution is

$$\psi_R = \gamma + \arccos\left(\frac{L\sin\beta}{\sqrt{(V\cos\beta)^2 + (V\tan\varphi_R)^2}}\right) \qquad (24)$$

$$\text{where} \quad \begin{cases} \cos\gamma = \frac{-V\cos\beta}{\sqrt{(V\cos\beta)^2 + (V\tan\varphi_R)^2}} \\ \sin\gamma = \frac{V\tan\varphi_R}{\sqrt{(V\cos\beta)^2 + (V\tan\varphi_R)^2}} \end{cases} \qquad (25)$$

The tracks of $v_{\infty out}$ are symmetric against P_3 axis as seen in Fig. 5. Therefore, examining the range of $-\pi/2 \le \varphi_R \le \pi/2$ suffices to know the entire solution space.
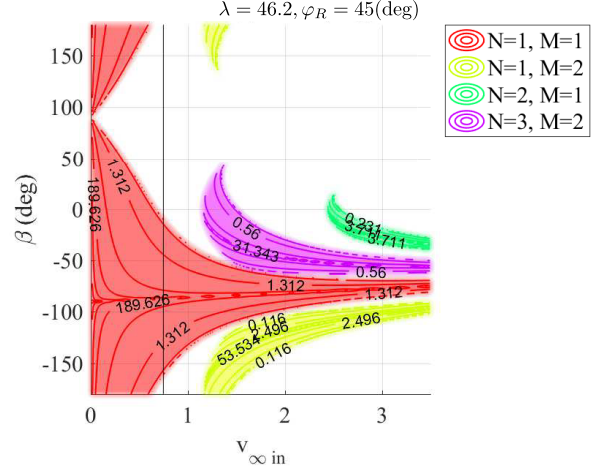
Once φ_R is specified, ψ_R is obtained by Eqs. (15) to (22). By providing two parameters φ_R and λ, one can judge if α_{max} is larger than α_{robust} for each incoming v_∞. Maps that represent possible synchronous orbits are obtained by this method, using v_∞ and β as independent variables. To understand the dependency on the parameters φ_R and λ, maps with $\lambda = 1$, 5, and 100 are shown for each $\varphi_R = 0$deg, 10deg, and 45deg in Fig. 7. In the figure, only the combinations of {N:M}={1:1}, {1:2}, {2:1}, and {3:2} are displayed. As λ becomes small, overlaps of reachable regions for different combination of {N:M} emerge. The maps with negative and positive φ_R are symmetric against a line of $\beta = 0$. This symmetry is in accordance with the symmetric behavior of $v_{\infty out}$ in P_1P_2 plane with respect to P_1 axis when β becomes negative. In the figure, we overlay contour lines on the reachable region that signify a non-dimensional altitude from a target body's surface at the periapsis. This altitude is computed from the non-dimensional version of Eq. (12). The information on the altitude is helpful in estimating necessary ΔV for the orbit insertion. As λ gets smaller, possible region for robust polar orbit insertion forms a closed shape as in the second row of the Fig. 7. The value of the contour is small in the area near the center of this closed shape.

In Fig. 6, detailed maps for Mars is shown. Values of v_∞ for Hohmann transfer from Earth is expressed as a black line. The values of λ and the characteristic v_∞ for Hohmann transfer from Earth are summarized in table 1. In the case of polar orbit insertion, necessary ΔV depends only on the altitude from the target body, given v_∞. By looking at the map, we can determine ideal v_∞ and β that satisfy the robust condition and small ΔV. Even in the other type of the orbit insertion, low altitude at periapsis generally contributes to the small ΔV for the insertion. Thus, the map also serves as a reference to estimate a desirable approaching condition.

4. Application to MMX Mission

Martian Moons eXplorer (MMX) mission is a sample return mission from one of the Martian Moons, Phobos. It is planned by JAXA to launch the probe in early 2020s. In the design of a trajectory that is tolerant to an orbit insertion failure, a key question is whether we can achieve robustness and small
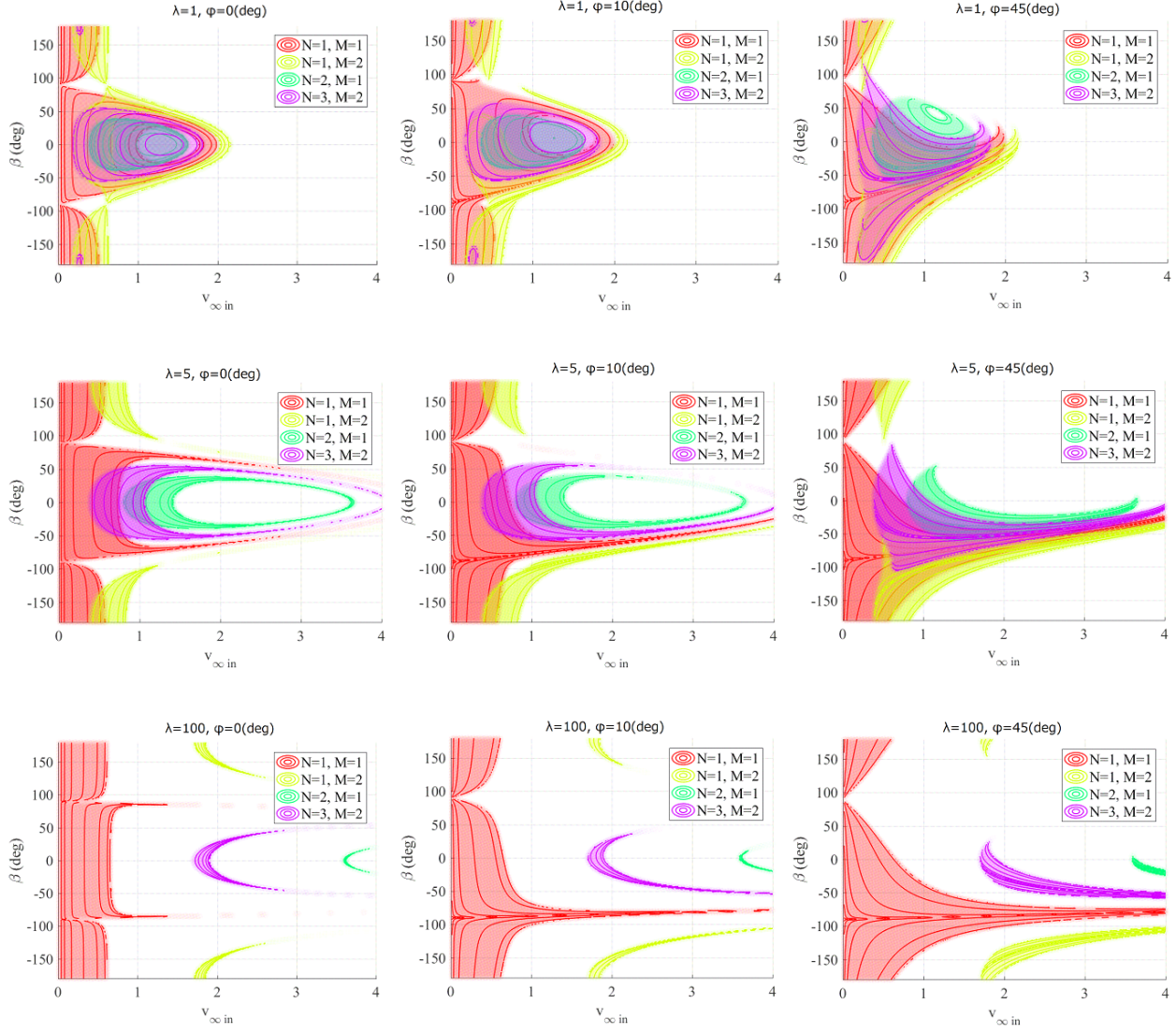
Fig. 7. Reachability of robust orbit insertion over v_∞ and angle β. Body associated parameter λ increases from top to bottom $(1, 5, 100)$. Geometric parameter φ_R increases from left to right $(0, 10\text{deg}, 45\text{deg})$.

ΔV for the entire mission at the same time. Since the explorer needs to visit Phobos, it executes multiple maneuvers to alter its trajectory. Necessary ΔV for the orbit insertion does not monotonously change according to the distance from Mars on the B-plane, which is a major difference with the polar orbit insertion. Except for this complexity in ΔV, the same computation is utilized.

From Fig. 6, we will see that a line showing the v_∞ for Hohmann transfer is on the region of 1:1 synchronous orbit when φ_R is large. Since MMX uses a trajectory like Hohmann transfer, we choose 1:1 synchronous orbit for the target of the robust orbit insertion. If the insertion maneuver fails, the probe can re-encounter Mars after one Martian year (1.88 Earth year).

An overview of the trajectory design is as follows.[8] In the preliminary design, the use of a chemical propulsion system and an electric propulsion system were investigated, and the plan to use the chemical propulsion system for the entire mission has been adopted. In the reported nominal condition, the spacecraft departs from Earth on August 23rd in 2022 and arrives at Mars about a year later. After the spacecraft arrives at SOI of Mars,

it performs three maneuvers for Mars orbit insertion (MOI) and transfers to the orbit of Phobos. They have explained the nominal sequence of MOI as follows.

- MOI1
  At the periapsis, MOI1 decelerate the explorer with respect to Mars and inject it into the elliptic orbit around Mars. The altitude at the periapsis is 500km from the ground and radius at the apoapsis is $40R_M$. R_M means the radius of Mars. This initial elliptic trajectory is designed so that its apoapsis is in the orbital plane of Phobos, which means the argument of periapsis ω regarding Phobos's orbital plane is either 180° or 0°.

- MOI2
  At the apoapsis where the orbital plane of Phobos and the orbital plane of the spacecraft intersect, MOI2 is performed. This maneuver changes its orbital plane to that of Phobos and lifts the altitude at the periapsis to the orbital radius of Phobos.

- MOI3
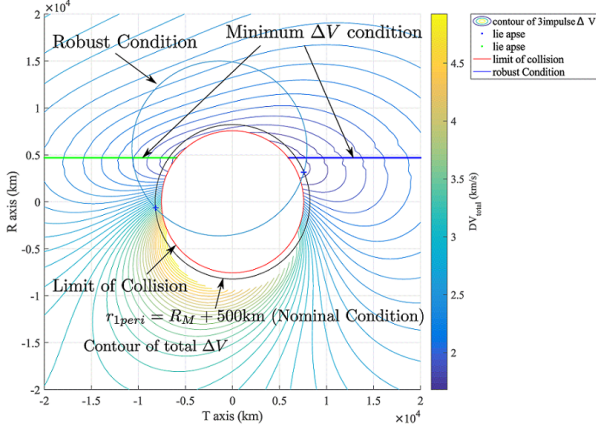 At the periapsis, MOI3 is applied and lowers the apoap-

Fig. 8. Conditions on B-plane for nominal launch and arrival case.

sis altitude. Ogawa et al. have explained that the merit of choosing the specific argument of periapsis ω is that it reduces ΔV for MOI2 since the plane change can be achieved when the spacecraft has the lowest velocity.[8]

For the computation of MOI, a similar sequence was adopted in this study. To enable the computation for any value of b and θ, we assumed that MOI2 was performed at either ascending or descending node. Except for MOI2, the scenario was same.

4.1. Robust Condition and ΔV on B-plane

Fig. 8 shows the contour of necessary total ΔV on the B-plane for the nominal launch case; also depicted are the nominal altitude (black circle), the robust MOI condition (blue circle), and the minimum ΔV condition (blue and green line). We define minimum ΔV condition as the condition where ω after MOI1 is either $0°$ or $180°$ In this case, the spacecraft accomplishes the plane change at the lowest speed.

If we fix the altitude at the periapsis to 500km, target point is on the black circle in the figure. An intersection of the blue line and the black circle is the potential solution if we do not take the robustness into account. When we give priority to the robust insertion, a target point is the intersection of the blue and black circle. In the latter case, additional ΔV is required. The amount

Table 2. Sample launch window

	Range of the window
Earth Departure	Aug. 21, 2022 - Sep. 3, 2022
Mars Arrival	Jul. 27, 2023 - Aug. 9, 2023

of drawback changes depending on the launch and arrival date. Therefore, we feedback the necessary drawback for the robust orbit insertion to the design of an interplanetary trajectory.

4.2. Determination of the Launch Window

Fig. 9 shows the porkchop plot to determine the feasible solutions. The blue lines, the red lines, and the black lines are the contour of total ΔV for MOI, the contour of minimum ΔV for MOI, and C_3 at Earth respectively. The altitude at MOI1 is fixed to $R_M + 500$km both in the robust and non-robust MOI. To decide a launch window, we filter out infeasible solutions. In the design of the nominal condition by Ogawa et al., mission requirements are defined as shown below.[8] We follow the same requirement for the trajectory design with robust MOI.

- C_3 at Earth is smaller than 18 km^2/s^2 .
- The declination of v_∞ at Earth satisfies $-30° \leq \delta \leq 30°$. This condition is required for the lunch from Tanegashima Space Center.
- The flight time is less than one year.
- There exists two weeks of the launch window that satisfies the above conditions.

In addition to the criteria considered in the nominal trajectory design, another condition that the extra ΔV to achieve robust MOI is no greater than 100m/s is added. Feasible solutions are in the white area.

We can secure a launch window that satisfies these conditions over the entire domain of two weeks by two weeks. For example, if we choose a new nominal launch window as shown in table 2, in the entire period, the extra ΔV is less than 76m/s. And if we choose a nominal launch date of Aug. 29, 2022 and arrival date of Aug. 6, 2023 in the window, the necessary extra ΔV is less than 1m/s.
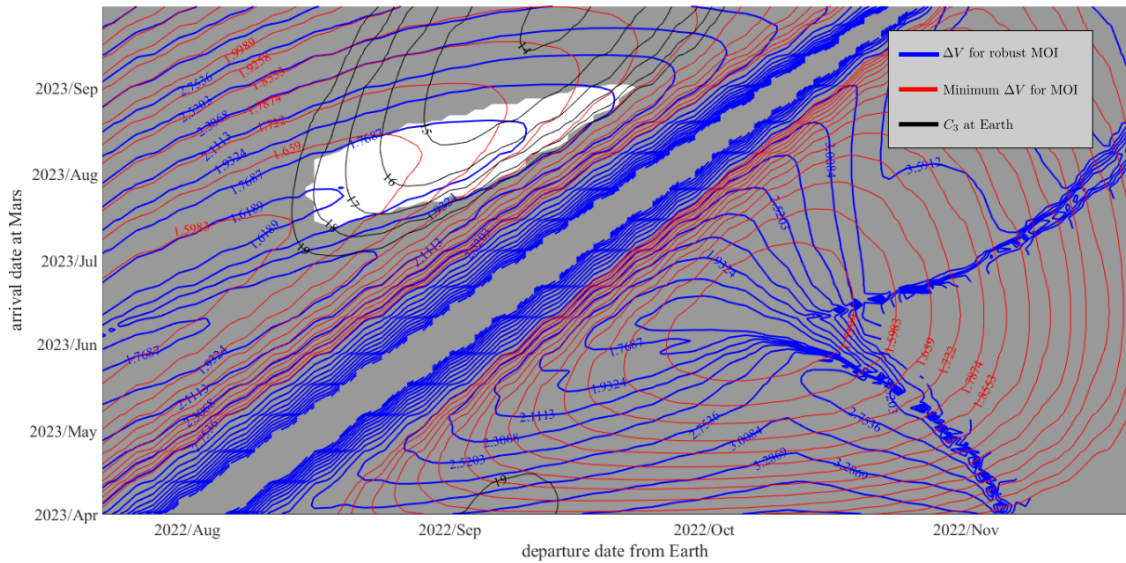

Fig. 9. Porkchop plot of minimum total ΔV (km/s) at MOI and total ΔV for robust MOI. Red lines represent the contour of minimum ΔV (km/s) at MOI. Blue lines represent the contour of total ΔV for the robust MOI. Black lines represent C_3(km^2/s^2) at Earth. Gray region has no feasible solution.

5. Conclusion

In this study, we investigated the general characteristics of the robust orbit insertion and its application to JAXA's MMX mission. Conclusions are as follows.

We established the analytical method to compute target points for the robust orbit insertion on the B-plane. The values of b and θ that satisfy the robust condition are obtained based on the geometry of the velocity vectors at the swing-by. Using the coordinate transformation, $v_{\infty out}$ was expressed by a single parameter ψ. For each ψ, the value of b is obtained through the computation of deflection angle α and the radius at periapsis r_{peri}. The angle θ that shows the direction of insertion is also computed by correlating the reference frame $O - P_1 P_3$ and the B-plane.

By properly choosing the scaling factors as R_p and $\sqrt{R_p^3/\mu_p}$, we showed that a maximum deflection angle achieved by the planet α_{max} and a necessary deflection angle for the robust polar orbit insertion α_{robsut} are classified by two parameters λ and φ_R. We showed that λ works as an index to show how difficult it is to deflect the trajectory at swing-by and φ_R works as a parameter to correlate the insertion direction on the B-plane.

General maps that show conditions on incoming v_∞ to achieve a robust polar orbit insertion were obtained for each set of two parameters λ and φ_R. We presented that by looking at the maps, desired approaching condition can be evaluated and mission planning would benefit from it.

The method of the robust orbit insertion is applied to the trajectory design of MMX mission and we confirmed that we can secure two weeks of launch window that satisfies the mission requirements that has extra ΔV for robust orbit insertion less than 100m/s.

References

1) Holdridge, M.: NEAR Shoemaker Spacecraft Mission Operations, *Johns Hopkins APL Technical Digest (Applied Physics Laboratory)*, 23(1)58-70, 2002.

2) Bell, J. and Mitton, J.: Asteroid rendezvous: NEAR Shoemaker's adventures at Eros. Cambridge University Press, 2002.

3) Hirose, C., Ishii, N., Yamamoto, T., Kawakatsu, Y., Ukai, C., Terada, H., and Ebara, M.: Orbital Design Strategies for Akatsuki Mission, *International Symposium on Space Technology and Science*, 2011.

4) Kawakatsu, Y., Yamamoto, M. and Kawaguchi, J.: Study on a Lunar Approaching Strategy Tolerant of a Lunar Orbit Injection Failure, *Trans. JSASS Aerospace Technology Japan*, **5**, 1 (2007), pp. 1–7.

5) Russell, R. and Ocampo, C.: Geometric Analysis of Free-Return Trajectories Following a Gravity-Assisted Flyby, *Journal of Spacecraft and Rockets*, **42**, 1, (2005), pp. 138–151.

6) Strange, N., Russell, R., and Buffingtonm B.: Mapping the V-Infinity Globe, *AAS Astrodynamics Specialist Conference, 07-277* (2007).

7) Kawakatsu, Y.: v_∞ direction diagram and its application to swingby design, 21st International Symposium on Space Flight Dynamics, Toulouse, France, Vol.1 , 2009.

8) Ogawa, N., Tsuda, Y. and Takei, Y.: Orbit Design for Martian Moons Exploration Mission, *JSASS Ukaren*, **60**, 1, (2016), (in Japanese).

9) Battin, H.: An Introduction to the Mathematics and Methods of Astrodynamics, AIAA Education Series, New York, 1987.